# Stress Analysis, Crack Propagation and Stress Intensity Factor Computation of a Ti-6Al-4V Aerospace Bracket using ANSYS and FRANC3D

by

Priscilla L. Chin

A Engineering Project Submitted to the Graduate

Faculty of Rensselaer Polytechnic Institute

in Partial Fulfillment of the

Requirements for the degree of

MASTER OF MECHANICAL ENGINEERING

Approved:

_____

Ernesto Gutierrez-Miravete, Project Adviser

Rensselaer Polytechnic Institute
Hartford, Connecticut

April 2011
(For Graduation May 2011)

# CONTENTS

# LIST OF SYMBOLS

E = Modulus of Elasticity (GPa)

ν = Poisson's Ratio (-)

ε = Strain (-)

u = Displacement (mm)

σ = Normal Stress (GPa)

τ = Shear Stress (GPa)

G = Shear Modulus (GPa)

Φ = Airy Stress Function (kN)

K = Stress Intensity Factor (GPa $\sqrt{mm}$ )

a = crack length (mm)

P = geometrical parameter depends on structural member and crack

@ = at

# LIST OF FIGURES

# LIST OF TABLES

# ACKNOWLEDGMENT

I would like to thank Professor Ernesto Gutierrez-Miravete for his guidance and advice throughout the course of this project, Valeriy Krutiy for providing information on resources and Michael R. Thomas for contributing his bracket geometry for this study.

## KEYWORDS

ANSYS

FRANC3D

Ti-6Al-4V

Corner crack

Crack propagation

Linear elastic fracture mechanics (LEFM)

Finite element method

Stress intensity factor

# ABSTRACT

The focus of this project is to investigate how a crack propagates and grows in a typical Ti-6Al-4V aerospace bracket. The finite element program ANSYS and the crack growth program FRANC3D were used to simulate crack growth and to compute the stresses and the stress-intensity factor. A specific bracket design was selected and a corner crack was investigated. This configuration was used since the engineers often detect this type of crack in brackets. The Von Mises stress near the crack tip is compared against the yield strength of the material. The Mode I stress-intensity factor is compared against the material's fracture toughness. The results show that the bracket can tolerate small cracks in the structure. The fatigue strength of the structure is recommended to be assessed in the future.

# 1. Introduction/Literature Review

Airliners progressively more demand for high performance and fuel-efficient aircrafts due to the increasing gasoline price. In order to meet the market needs, original equipment manufacturers are developing smaller and lighter aircraft engines. Industry analysts are expecting the engine components in the next decades to be very space efficient. As a result, light but high strength materials are very valuable and competitively sourced to reduce weight and cost in manufacturing aircraft engine.

Aero engine designers design brackets in various shapes and sizes for mounting bleed air ducting, starter air duct, fuel lines and hydraulic lines to the engine core. One can find more than one hundred mounting points in an engine. Many of the ducting supports have the shapes of L, T and Z (multiple bends) to accommodate multiple tubes in the tight space found in an aircraft engine. In general, the bracket thickness ranges from .125 to .500 inch because the brackets not only must be thin to reduce weight and cost, but also must be functional and serve its purposes in the extreme environment, e.g. extremely high temperature, combination of vibration load, bending moment and maneuver load. Any crack found in a bracket may cause the ducting to become unstable during a mission, and thus induce high cycle fatigue load on the overall major structures and shorten the structures life. From the economic standpoint, it is a cost saving strategy to replace brackets before they are completely damaged due to replacing broken brackets mitigates the risk of damaging other major components, such as the ducting, which are more costly to replace. Besides, replacing a bracket before it completely breaks can avoid many engineering catastrophes and save many lives. On the other hand, knowing the fatigue life of a component, a mechanic can plan the inspection interval accordingly.

Nickel-based alloys such as Inconel 718 and Inconel 625 are widely used in aerospace industry for ducting and brackets. However, according to Honnorat [2], only titanium alloys could satisfy the requirement and the increasing demand for high strength per weight materials that needed for a wide range of components. According to the unknown author on World Wide Web, Wikipedia [4], many aircraft use titanium due to their high tensile strength to density ratio, high corrosion resistance, fatigue resistance, high crack resistance, and ability to withstand moderately high temperatures without creeping.

Honnorat wrote in his paper in 1996 that jet engine designers use more and more titanium in both commercial and military projects, attaining contents as high as 30% of the total engine mass in the commercial and 40% in the military projects [2]. His statistic is consistent with recent data found on internet that about two thirds of all titanium metal produced is used in aircraft engines and frames [4]. In fact, many engine applications that use titanium include rotors, compressor blades, hydraulic system components, and nacelles. Among all the titanium-based alloys, according to Immarigeon et al, Ti-6-4 is by far the most widely used, accounting for almost half of all titanium used in aircraft [3]. Besides, he also mentioned Ti-6-2-4-2 is the other type of titanium-based alloy widely used in engines, which is stronger and more creep-resistant than Ti-6-4 [3]. According to Immarigeon et al [3], titanium-based alloys are widely used in engine applications because the material can increase the strength-to-weight ratio in structures and provide heat resistance with weight savings. The materials behavior under aggressive environment as well as impact loads make them attractive for aeroengine applications [2]. Their relatively low density decreases the magnitude of vibration problems [2]. However, the significant weight savings permitted by these titanium application developments generates specific drawbacks that needed particular technological developments. Among the most important concerns are the brittle inclusions, which are difficult to detect by non-destructive testing, and can initiate cracks and an early failure of the structures [2]. Materials imperfections due to manufacturing process, for example, voids and impurities develop flaws that can cause a material to become weak.

## 2. Problem Statement

Cracks often develop in the corners of a structural member due to high stress concentration factor in those areas. If one can calculate the rate of crack growth, an engineer can schedule inspection accordingly and repair or replace the part before failure happens. Moreover, being able to predict the path of a crack helps a designer to incorporate adequate geometric tolerance in structural design to increase the part life. While producing durable, reliable and safe structures are the goals of every aerospace component manufacturer, there are technical challenges that are not easy to be solved. Given limited engine design space, engineers strive to optimize bracket geometry to produce high efficient and high performance engines that will operate at minimum weight and cost. Engineers often look to shave materials from bracket and design the thinnest possible brackets. Benefits from this approach include reduced weight, and smaller probability of encountering brittleness inducing microstructural defects. The focus of this paper is to investigate the corner crack growth in a titanium-based alloy bracket. This paper will examine the stresses near the crack tip, compute the stress-intensity factors and compare it against material toughness to determine the influence of the crack on the bracket.

# 3. Theory

## 3.1 Linear Elastic Fracture Mechanics (LEFM)

For any homogeneous and isotropic material, stress surrounding the crack tip is often analyzed assuming linear elastic material behavior [5]. The method of linear elastic fracture mechanics assumes the plastic region near crack tip is much smaller than the dimensions of the crack and the structural member. This is a very important concept, scientists and engineers call it small-scale yielding [5], for simplifying the stress analysis near crack tip. Assuming the geometry has very small displacement and the material is elastic, homogeneous and isotropic. The governing equations for linear elastic analysis in 2-D are

The strain-displacement relationships:

$$\varepsilon_{xx} = \frac{\partial u_x}{\partial x} \qquad \varepsilon_{yy} = \frac{\partial u_y}{\partial y} \qquad \varepsilon_{xy} = \frac{1}{2}\left[\frac{\partial u_x}{\partial y} + \frac{\partial u_y}{\partial x}\right] \qquad \textbf{Eq. (1) – (3)}$$

The stress-strain relationships:

i. For plane strain, where $\varepsilon_{zz} = \varepsilon_{xz} = \varepsilon_{yz} = \tau_{xz} = \tau_{yz} = 0$ **Eq. (4)**

$$\sigma_{xx} = \frac{E}{(1+\nu)(1-2\nu)}\left[(1-\nu)\varepsilon_{xx} + \nu\varepsilon_{yy}\right] \qquad \textbf{Eq. (5)}$$

$$\sigma_{yy} = \frac{E}{(1+\nu)(1-2\nu)}\left[(1-\nu)\varepsilon_{yy} + \nu\varepsilon_{xx}\right] \qquad \textbf{Eq. (6)}$$

$$\tau_{xy} = 2G\varepsilon_{xy} = \frac{E}{1+\nu}\varepsilon_{xy} \qquad \textbf{Eq. (7)}$$

$$\sigma_{zz} = \nu(\sigma_{xx} + \sigma_{yy}) \qquad \textbf{Eq. (8)}$$

ii. For plane stress, where $\sigma_{zz} = \varepsilon_{xz} = \varepsilon_{yz} = \tau_{xz} = \tau_{yz} = 0$ **Eq. (9)**

$$\sigma_{xx} = \frac{E}{1-\nu^2}\left[\varepsilon_{xx} + \nu\varepsilon_{yy}\right] \qquad \textbf{Eq. (10)}$$

$$\sigma_{yy} = \frac{E}{1-\nu^2}\left[\varepsilon_{yy} + \nu\varepsilon_{xx}\right] \qquad \textbf{Eq. (11)}$$

$$\tau_{xy} = 2G\varepsilon_{xy} = \frac{E}{1+\nu}\varepsilon_{xy} \qquad \textbf{Eq. (12)}$$

$$\varepsilon_{zz} = \frac{-\nu}{1-\nu}(\varepsilon_{xx} + \varepsilon_{yy}) \quad \textbf{Eq. (13)}$$

The equilibrium equations:

$$\frac{\partial \sigma_{xx}}{\partial x} + \frac{\partial \tau_{xy}}{\partial y} = 0 \quad \textbf{Eq. (14)}$$

$$\frac{\partial \sigma_{yy}}{\partial y} + \frac{\partial \tau_{xy}}{\partial x} = 0 \quad \textbf{Eq. (15)}$$

and the compatibility equation:

$$\left[\frac{\partial^2}{\partial x^2} + \frac{\partial^2}{\partial y^2}\right](\sigma_{xx} + \sigma_{yy}) = 0 \quad \textbf{Eq. (16)}$$

The Airy stress function, $\Phi$, can satisfy all the governing equations and is used to derive the stress field near the crack tip.

$$\phi = \frac{K_I}{3\sqrt{2\pi}} r^{3/2}\left(\cos\frac{3\theta}{2} + 3\cos\frac{\theta}{2}\right) \quad \textbf{Eq. (17)}$$

$$\frac{\partial^4 \phi}{\partial x^4} + 2\frac{\partial^4 \phi}{\partial x^2 \partial y^2} + \frac{\partial^4 \phi}{\partial y^4} = 0 \quad \textbf{Eq. (18)}$$

Solving Eq. (18) yields the stress fields for Mode I as

$$\sigma_x = \frac{K_I}{\sqrt{2\pi r}}\cos\frac{\theta}{2}\left(1 - \sin\frac{\theta}{2}\sin\frac{3\theta}{2}\right) \quad \textbf{Eq. (19)}$$

$$\sigma_y = \frac{K_I}{\sqrt{2\pi r}}\cos\frac{\theta}{2}\left(1 + \sin\frac{\theta}{2}\sin\frac{3\theta}{2}\right) \quad \textbf{Eq. (20)}$$

$$\tau_{xy} = \frac{K_I}{\sqrt{2\pi r}}\cos\frac{\theta}{2}\cos\frac{3\theta}{2}\sin\frac{3\theta}{2} \quad \textbf{Eq. (21)}$$

$$\sigma_z = \nu(\sigma_x + \sigma_y) \quad \textbf{Eq. (22)}$$

$$\tau_{xz} = \tau_{yz} = 0 \quad \textbf{Eq. (23)}$$

and the displacement fields are

$$u = \frac{K_I}{G}\sqrt{\frac{r}{2\pi}}\cos\frac{\theta}{2}\left(1 - 2\nu + \sin^2\frac{\theta}{2}\right) \quad \textbf{Eq. (24)}$$

$$v = \frac{K_I}{G}\sqrt{\frac{r}{2\pi}}\sin\frac{\theta}{2}\left(2 - 2\nu - \cos^2\frac{\theta}{2}\right) \quad \textbf{Eq. (25)}$$

$$w = 0 \quad \textbf{Eq. (26)}$$

The coordinates (r,θ) for the stress components are shown in Figure 1

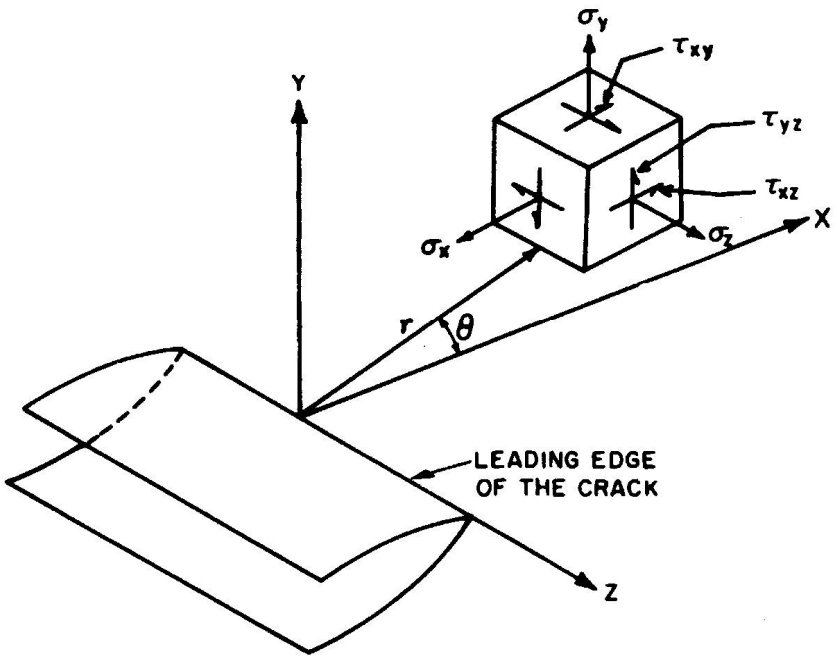


**Figure 1 Coordinate systems for the stress components [5].**

## 3.2 Calculation of Stress Intensity Factors (SIF) using the Finite Element Method

When a crack exists in a structure, stress is concentrated at the tip but the stress concentration do not account for the fracture behavior at the tip of a crack because as the radius of the curvature of the crack tip approaches zero, the stress level could become infinity, which is not a real property of a loaded structure. As an alternative to describe the structural strength at the crack tip appropriately, the stress-intensity factor, K, is a parameter to characterize "the stress field ahead of a sharp crack in a test specimen or a structural member" [5]. The parameter, K, is related to the nominal stress level (σ) in the structural member and the size of the crack (a), and has units of $(GPa\sqrt{mm})$. In general, the relation is represented by:

$$K = \sigma \sqrt{a}\ P \qquad \textbf{Eq. (27)}$$

where P is a geometrical parameter depends on the structural member and crack. According to Barsom [5], "all structural members or test specimens that have flaws can

be loaded to various levels of K. This is analogous to the situation where unflawed structural or mechanical members can be loaded to various levels of stress, σ".

The stress field near crack tips can be categorized as Mode I: opening mode, Mode II: sliding and Mode III: tearing, which each of them is characterized by a "local mode of deformation" as illustrated in Figure 2. The opening mode, I, is related to local displacement in which the crack surfaces move directly apart (symmetric with respect to the x-y and x-z planes). The sliding mode, II, is related with local displacement in which the crack surfaces slide over one another perpendicular to the leading edge of the crack (symmetric with respect to the x-y plane and skew-symmetric with respect to the x-z plane). The tearing mode, III, is related with local displacement in which the crack surfaces slide with respect to one another parallel to the leading edge (skew-symmetric with respect to the x-y and x-z planes). Although these three modes can be superposed to "describe the most general case of crack tip deformation and stress fields" [6], Mode I is the primary focus of this paper.

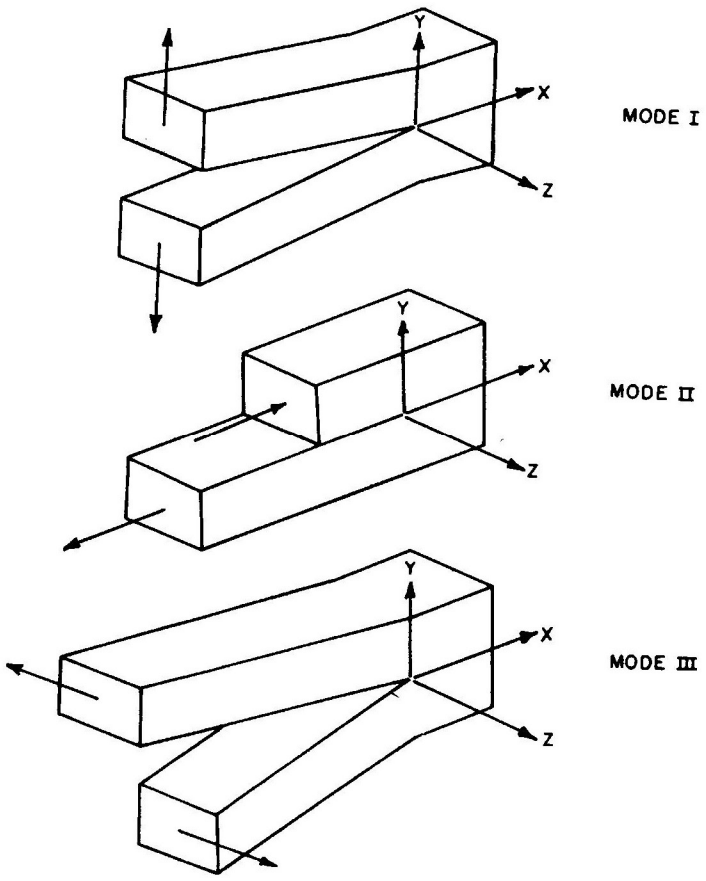


**Figure 2 The three basic modes of crack surface displacements [5].**

In general, stress-intensity factor depends on the stress induced on a structure, the crack size and the geometry of the crack. The stress-intensity factor equation for an embedded circular crack is given by [6]:

$$K_I = \frac{\sigma\sqrt{\pi a}}{\phi}\left(\sin^2\beta + \frac{a^2}{c^2}\cos^2\beta\right)^{1/4} \qquad \textbf{Eq. (28)}$$

If the crack occurs at the corner of a beam, as shown in Figure 3, the $K_I$ expression would be [5]:

$$K_I = (1.12)(1.12)\frac{2}{\sqrt{\pi}}\sigma\sqrt{a} \qquad \textbf{Eq. (29)}$$

1.12 is the free surface correction factor, which is added for every free surface at which a crack might originate. $K_I$ is increased by $(1.12)^2$ [5] because there are two free-surface corrections for a corner crack.

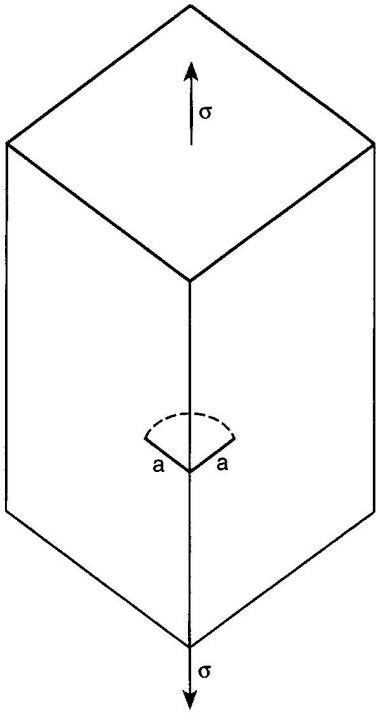


**Figure 3 Circular corner crack [5].**

The finite element method was used to calculate the stress intensity factor due to the complexity of the bracket geometry and boundary conditions. Since a singularity exists as r approaches zero, see Eq.(19), Eq.(20) and Eq.(21), finite element codes must meet two requirements to resolve the singular stress at the crack tip. The first requirement is the element size: the new elements used to populate the crack region must be smaller than the existing mesh to calculate the stress-intensity factors accurately. However, the new elements must be large enough to address singularity at the crack tip. The second requirement is the element number: the number of elements around the crack tip influences the circumferential stress distribution. In general, the stress result is more accurate with more elements; but the results quality is compensated if the crack tip is over crowded with high aspect ratio elements. In order to meet the requirements by generating a smooth transition from the tip of the crack to the unmodified mesh, the FRANC codes insert "a rosette of crack-tip elements" that can be subdivided automatically and repeatedly into triangular and quadrilateral elements, see Figure 4 [10].

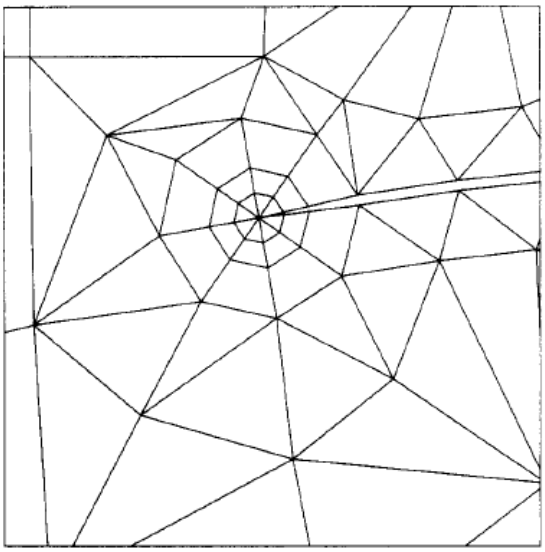

**Figure 4 Crack-tip elements [10].**

# 4. Methodology

Engineers strive to optimize bracket geometry by designing the thinnest possible brackets because this approach not only reduce engine weight but also reduce the risk of brittle structure often found in bulk materials. Being able to determine the rate of crack growth, an engineer can schedule inspection accordingly and repair or replace the part before failure happens. Being able to predict the path of a crack helps a designer to incorporate adequate geometric tolerance in structural design to increase the part life. The methodology used to investigate the mechanics of crack propagation consists of the following steps:

- CAD model creation
- Elastic stress analysis of the uncracked body
- Flaw implementation
- Crack propagation
- Elastic stress analysis of the cracked body
- Calculation of stress intensity factor
- Interpretation of results

Carter, Wawryznek and Ingraffea have developed a time saving method to replace the tedious and repetitive work of crack growth simulation and coded it in the computer program FRANC3D [8]. However, this code has limited stress analysis capability and must be used in conjunction with a finite element method program, such as ANSYS.

The software used for stress analysis in this study is ANSYS Release 11.0. It is a popular code used by many experts in various industries for finite element analysis. The author chose ANSYS Release 11.0 for its compatibility with FRANC3D Version 5.0. Dr. Paul Wawryznek developed the early FRANC codes in Cornell Fracture Group to simulate the process of nucleation and crack propagation in a structure; and to compute the stress intensity factor. Today, his students in the same group continue to research and update the codes [1].

## 4.1 CAD Model and Material Properties

Michael Thomas [7] contributed the bracket geometry used in his prior work to this study. It is a triangular hollow bracket with the 101.6 mm in height, 203.2 mm in width

and 10 mm in thickness. In addition, the boundary condition chosen by Thomas for his optimum bracket research was applied to the bracket in this study. At the base of the bracket, one end is clamped in all degree of freedom, while the other end is a slider. The bracket is pulled downward from the mid-section of the base and is pulled to the right at the top corner (see Figure 5).

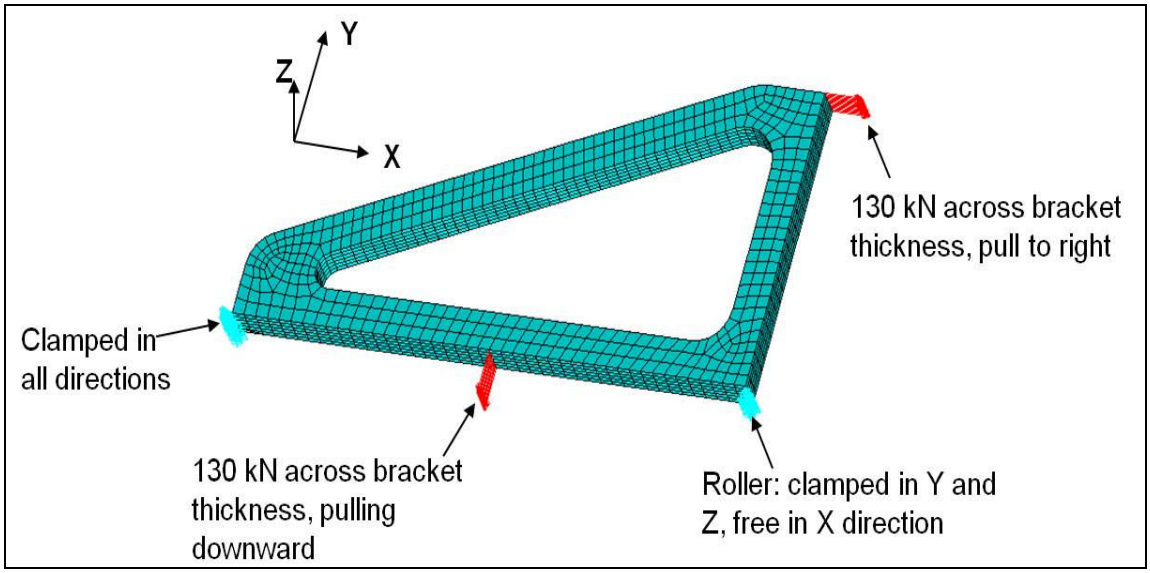


**Figure 5 The boundary conditions of the unnotched bracket.**

Among all the titanium-based alloys, according to Immarigeon et al [3], Ti-6Al-4V is by far the most widely used, accounting for almost half of all titanium used in aircraft because the material can increase the strength-to-weight ratio in structures and provide heat resistance with weight savings. However, the significant weight savings permitted by these titanium application developments generate specific drawbacks that need particular technological developments. Among the most important concerns are brittle inclusions, which are difficult to detect by non-destructive testing, can initiate cracks and produce early failure of the structures [2]. Materials imperfections due to manufacturing process, for example, voids and impurities can develop flaws that may cause the material to become weak. For those reasons, the material chosen in this study is Titanium-6Al-4V and the properties are summarized in Table 1.

| Material Properties | | Comments |
|---|---|---|
| Density | 4.43 g/cc | |
| Tensile Strength, Ultimate | 1170 MPa | |
| Tensile Strength, Yield | 1100 MPa | |
| Elongation at Break | 10.00% | |
| Modulus of Elasticity | 114 GPa | Average of tension and compression |
| Compressive Yield Strength | 1070 MPa | |
| Notched Tensile Strength | 1550 MPa | $K_t$ (stress concentration factor) = 6.7 |
| Poisson's Ratio | 0.33 | |
| Fatigue Strength | 160 MPa | $K_t$ (stress concentration factor) = 3.3 |
| | @ no. of cycles 1.00e+7 | |
| | 700 MPa | Unnotched |
| | @ no. of cycles 1.00e+7 | |
| Fracture Toughness | 43.0 MPa-m½ | |
| Shear Modulus | 44.0 GPa | |
| Shear Strength | 760 MPa | Ultimate shear strength |

**Table 1 Material properties of Titanium-6Al-4V.**

## 4.2 Analysis Procedure

The first step of the analysis was to perform finite element elastic stress analysis on the unnotched bracket to determine the stress distribution across the entire bracket and identify the weakest point or high stress regions. Michael R. Thomas, who created the geometry for his research paper, contributed the bracket CAD file [7]. The bracket CAD file was in parasolids format, which is compatible with ANSYS. The bracket was then meshed in the ANSYS environment using 20-noded brick elements (Solid95) since this is the only type of element compatible with FRANC3D. The finite element model of the unnotched bracket had 2828 elements and 12342 nodes. The author also constructed the Ti-6Al-4V stress-strain curve based on the data in Table 1 using the ANSYS graphic user interface (GUI). After the author applied boundary conditions to the bracket as shown in Figure 5, she set ANSYS to perform a single load step static stress analysis on the bracket. Once the calculation was completed, the ANSYS postprocessor was used to identify the high stress region for introduction of the initial crack. Finally, ANSYS wrote a database DB file (.cdb), which was subsequently used as input to FRANC3D for crack growth analysis.

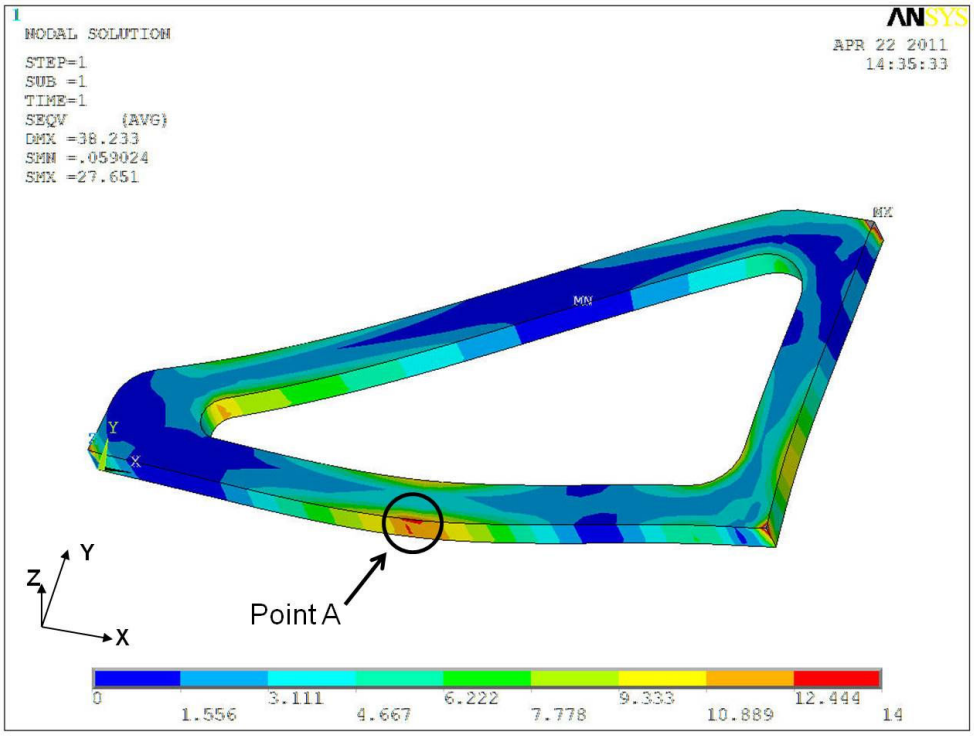


**Figure 6 Stress distribution of the unnotched bracket (Von Mises).**

Step two of the analysis consisted of introducing an initial crack in the structure by creating the basic geometry of the crack. After opening in FRANC3D, the .cdb file produced by ANSYS in step one, an initial crack was inserted in the structure by creating a half-millimeter radius circular region, and positioning it at the weakest point identified in step one, see point A in Figure 6. The stress singularity at the top right corner of the bracket was due to point load effect, so its influence on the structure was not real and was not considered. One quarter of the circular crack was inserted at the edge to simulate the corner crack. This method was proposed by Nishioka [9]. After that, FRANC3D automatically generated finer elements locally around the inserted crack. To ensure the new node pattern was not predetermined by the old mesh, FRANC3D erased the old elements around the crack before inserted new elements of the proper shape and number. Subsequently, FRANC3D filled the area between the new elements and the unmodified portion of the mesh with transition elements [10]. Finally, the FRANC3D GUI was used to create a new text file (.macro) readable by ANSYS for subsequent stress analysis.

Step three consisted of performing elastic stress analysis of the notched bracket produced by FRANC3D using ANSYS. The macro file contains all the procedures for running the load step analysis and post-processing the results. Therefore, once the notched bracket from step two was imported into ANSYS by reading in the text file (.macro) and executed, a results file (.dtp) for the cracked body was generated. This is a FRANC3D readable binary file.

Step four of the analysis consisted of using FRANC3D to compute the stress-intensity factor and to further extend the crack based on the node displacements at the crack tip obtained from the results file (.dtp). The direction of crack propagation is determined by a "propagation angle criterion" [10] and the calculated stress-intensity factors. The program uses "a heuristic algorithm" to determine the new mesh pattern. Wawrzynek described the process of stress-intensity factor computation and the mechanism of crack propagation in his paper, "The crack is then extended and a rosette of quarter-point singular elements are placed around the new crack-tip" [10]. In each iteration, the author used the default value for the crack tip size. Then the program computed the stress-intensity factor based on the stress result (.dtp) and the new crack length. The new crack length is calculated based on a polynomial series, where the variable of the series is the displacement of the node at the crack tip [8]. In this study, the author repeated steps three and four twice to examine the partial propagation of the crack. However, the process can be continued and the crack propagated and reanalyzed until a desired cumulated crack length is achieved.

# 5. Results and Discussion

There must be at least six elements across the bracket thickness to insert new crack elements in FRANC3D, for this reason, brick elements were used to ensure enough elements were present across the thickness while keeping the total number of elements in the geometry small. However, since FRANC3D deployed a "tetrahedral volume meshing algorithm" [8] to implement and propagate the initial crack, the program did a one-time remesh of the entire bracket geometry turning brick elements into tetrahedral elements. In the subsequent crack growth procedure, FRANC3D locally remeshed the elements around the crack; therefore, the area around the crack always had a finer mesh than the area further away from the crack. In general, once the geometry was populated with tetrahedral elements, areas far from the crack preserved the same node pattern between load steps. This is shown in Figure 7. After two load steps of crack propagation, about 24223 elements were added to the unnotced finite element model. Table 2 summarizes the number of elements and nodes in each finite element model.

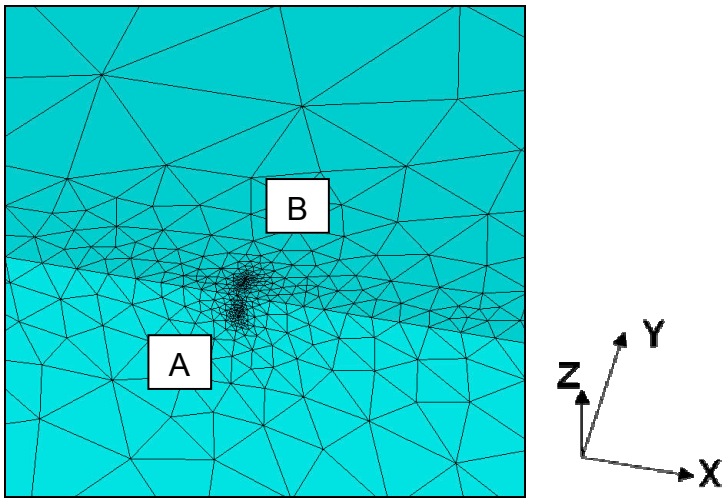


(7a) Initial crack.

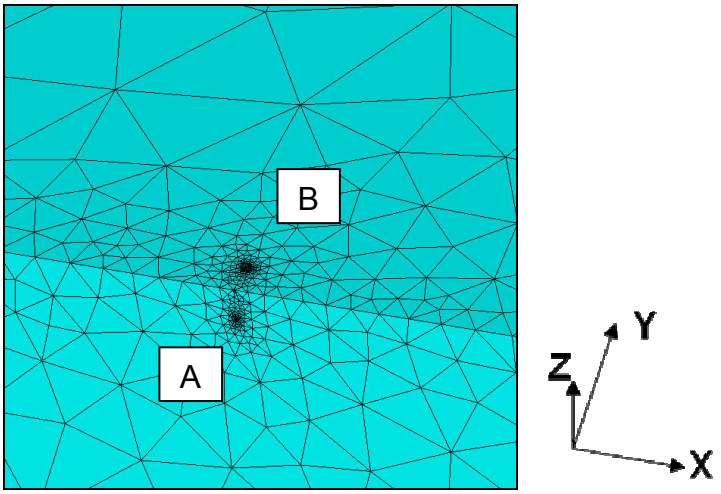


(7b) Propagated crack after two load cycles.

**Figure 7 Corner crack propagation.**

| Description of Bracket FEM | Number of Elements | Number of Nodes |
|---|---|---|
| Unnotched | 2828 | 12342 |
| Initial Crack | 26256 | 43390 |
| Propagated Crack After 2 Load Steps | 27051 | 45139 |

**Table 2 Number of elements and nodes.**

## 5.1 Stress Field around Initial Crack

Figure 8 shows the computed Von Mises stress field surrounding the initial crack at the end of step three in the analysis. The maximum value near the crack tip is 56.2 GPa. This value is above the yield stress of the material.

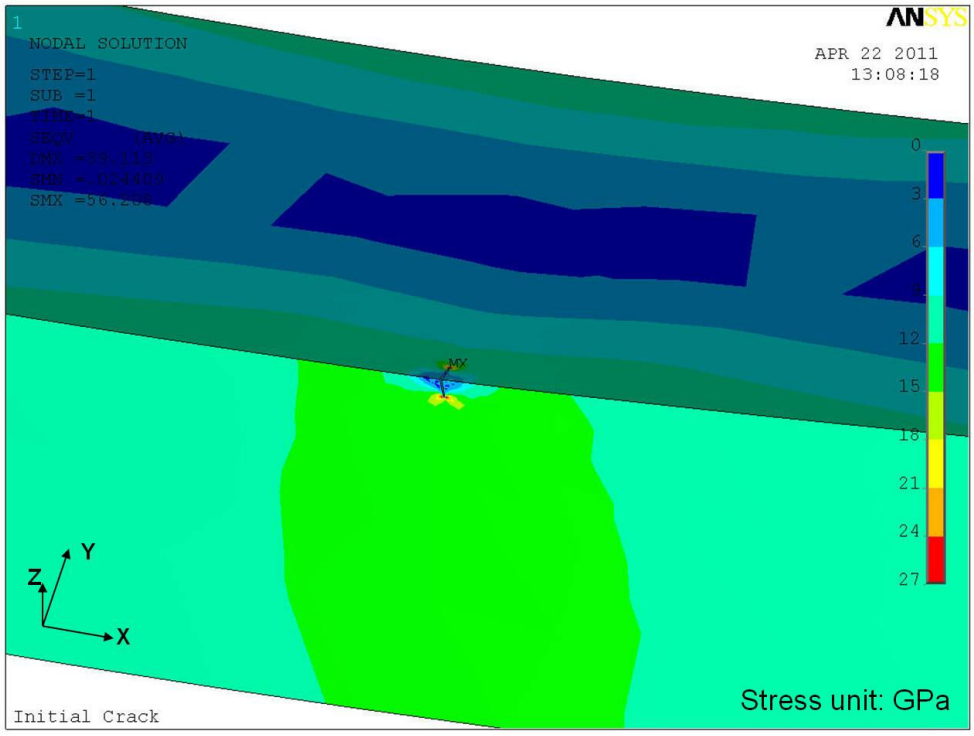


**Figure 8 Stress field around initial crack.**

## 5.2 Stress Field around Propagated Crack

Figure 9 shows the stress field surrounding the propagated crack after step four was repeated twice in the analysis. After two load steps of crack propagation, the maximum value near the crack tip is 133.3 GPa. It is still above the yield stress.

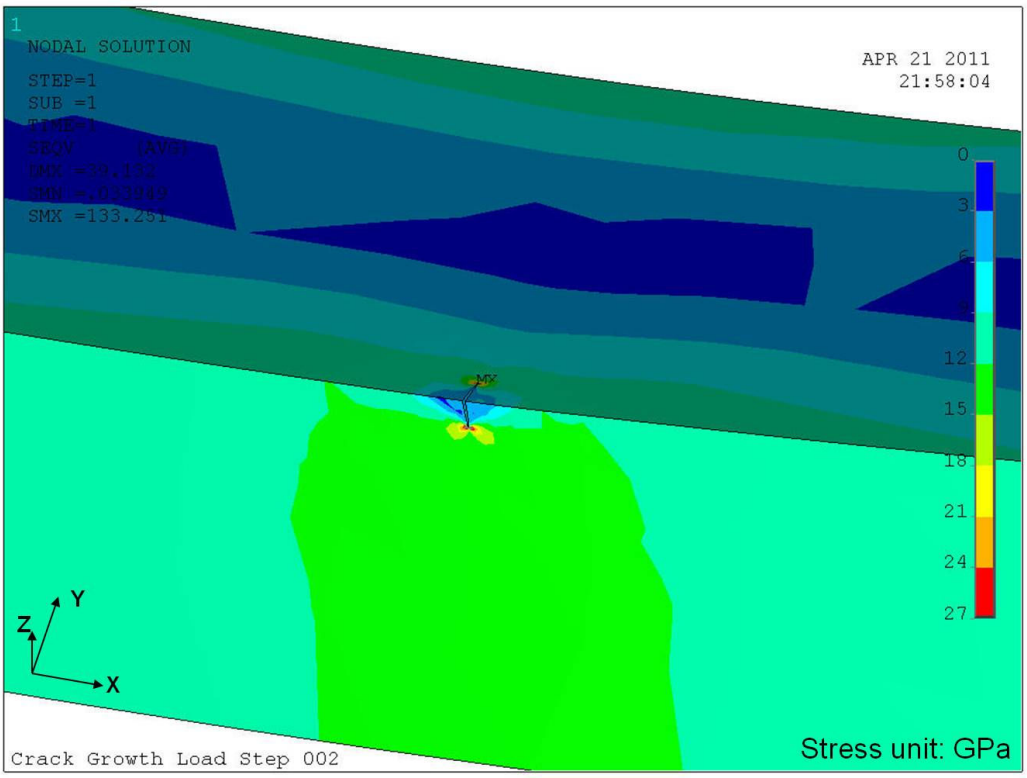


**Figure 9 Stress field around propagated crack after two load cycles.**

## 5.3 Stress Intensity Factor

Figure 10 shows the Mode I stress-intensity factors as a function of the normalized distance between the two extremities of the crack. The highest value (14.8 $GPa\sqrt{mm}$) occurs at point A after two load cycles. This value is below the material's fracture toughness. The analysis results also show that the Mode I stress-intensity factor at one end of the crack (point A) is higher than at the other end, see Figure 10, since point A is at the face where the force is directly applied. The magnitudes of Mode I stress-intensity factor increase as the crack propagates further during subsequent load steps. The results can be validated by the methods proposed by Nishioka [9], but this was not done in this report.

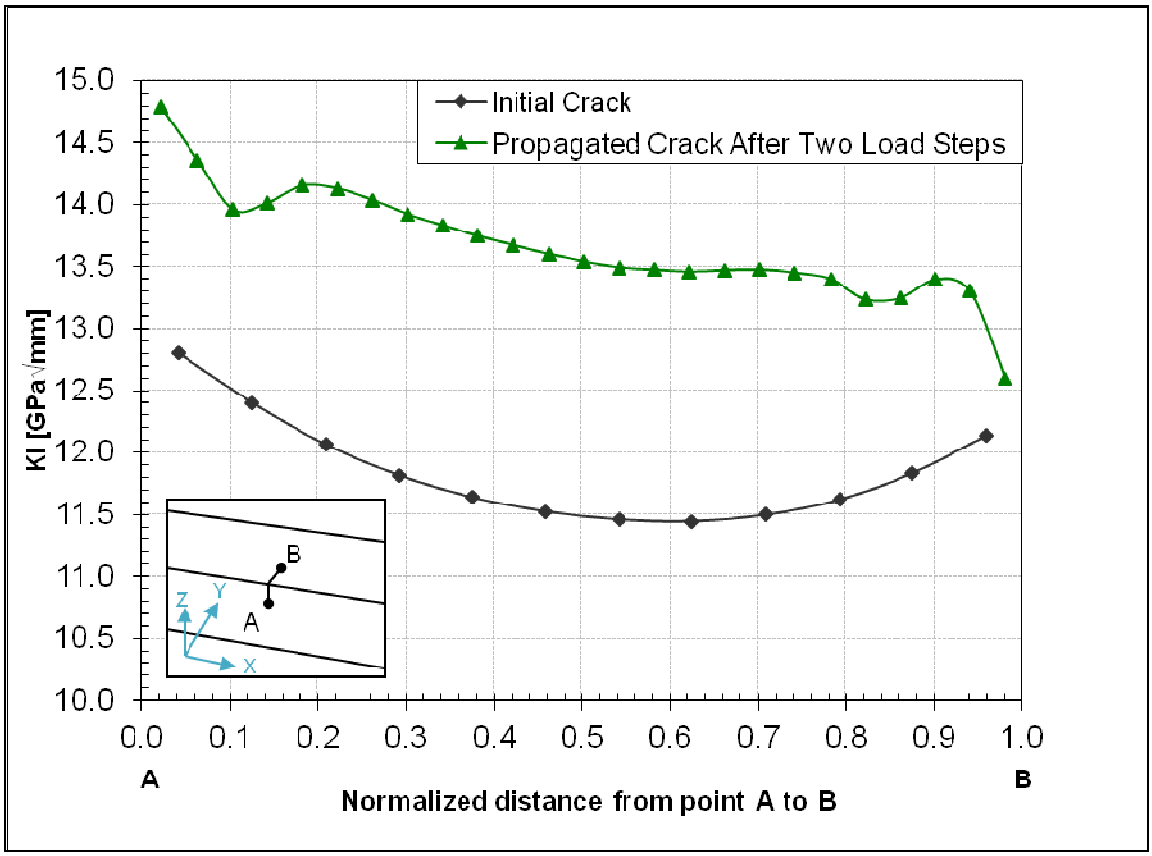


**Figure 10 Mode I stress-intensity factors.**

# 6. Conclusions

This project investigated the process of crack propagation and the resulting stress distribution in a typical Ti-6Al-4V aerospace bracket using ANSYS and FRANC3D. The behavior of corner cracks was studied since this type of flaw is most frequently encountered in practice. The first step of the analysis consisted of using ANSYS to perform elastic stress analysis on an existing unnotched bracket to identify the high stress regions. In step two, the unnotched model was imported to FRANC3D, an initial crack of simple geometry was introduced and several ANSYS files were created with a remeshed finite element structure around the crack. Step three of the analysis consisted of using ANSYS to perform elastic stress analysis of the notched bracket produced by FRANC3D. In step four, FRANC3D was used again to compute the stress-intensity factor and to further extend the crack. Steps three and four were then repeated twice to obtain the results reported in this paper. For the model of corner cracks, the results show that the Von Mises elastic static stress is above the yield strength for the two load cycles considered in this study. The crack length after two load cycles was 0.72 mm, which was an increment of 0.22 mm from the initial length (0.50 mm). The Mode I stress-intensity factors for the cracked model are below the material's fracture toughness. Therefore, it appears that the bracket can tolerate small corner cracks in the structure.

# 7. References


[1] Unknown. FRANC3D & ANSYS Tutorial. September 2010. http://www.fracanalysis.com/Franc3D_Documentation (accessed February 5, 2010).

[2] Honnorat, Yves. "Issues and breakthrough in manufacture of turboengine titanium parts." Materials Science and Engineering A213, 1996: 115-123.

[3] Immarigeon, J-P., Holt, R.T., Koul, A.K., Zhao, L., Wallace, W. and Beddoes, J.C., Lightweight Materials for Aircraft Applications, NRC Institute for Aerospace Research, 1995.

[4] Unknown. Titanium. n.d. http://en.wikipedia.org/wiki/Titanium (accessed January 12, 2011).

[5] Barsom, John M. and Rolfe, Stanley T., Fracture and Fatigue Control in Structures: Application of Fracture Mechanics, Philadelphia, 1999.

[6] Paris, C.P. and Sih, G.C., "Stress Analysis of Cracks," in Fracture Toughness Testing and Its Applications, ASTM STP 381, American Society for Testing and Materials, Philadelphia, 1965.

[7] Thomas, Michael R., Shape and Topology Optimization of Brackets using the Level Set Method, Master of Engineering in Mechanical Engineering Project Report, Hartford CT, 2010.

[8] Carter, B.J., Wawrzynek, P.A. and Ingraffea, A.R., Automated 3D Crack Growth Simulation, Cornell Fracture Group, 2003.

[9] Nishioka T. and Atluri S.N., Analytical Solution For Embedded Elliptical Cracks, And Finite Element Alternating Method For Elliptical Surface Cracks, Subjected to Arbitrary Loadings, Engineering Fracture Mechanics Vol. 17, No.3, pp. 247-268, 1983.

[10] Wawrzynek, P.A. and Ingraffea, A.R., An Interactive Approach To Local Remeshing Around A Propagating Crack, Finite Elements in Analysis and Design 5 (87-96), 1989.

# 8. Appendices

## 8.1 ANSYS Input Files

### 8.1.1 Initial Crack (.macro)

```
/BATCH,LIST
/CWD,'C:\Documents and Settings\m309112\My Documents\ESP Graduate
Schools\4-21-11'
/FILNAME,'Initial_crack',0
/CONFIG,NOELDBW,1
/INPUT,'C:\Documents and Settings\m309112\My Documents\ESP Graduate
Schools\4-21-11\Initial_crack','cdb'
/PREP7
save
/COM, select everything and solve
allsel,all,all
/SOLU
eqslv,PCG,1.0e-8
/COM, input solve commands
/INPUT,'C:\Documents and Settings\m309112\My Documents\ESP Graduate
Schools\4-21-11\Initial_crack','lsm'
/PREP7
/FORMAT,9,G,26,15
/POST1
/GRAPHICS,off
RSYS,0
/COM, reread results
/COM, INRES,ALL
/COM, FILE,'Initial_crack','rst'
/COM, output displacements, temperatures, crack surface pressures to
file
/INPUT,'C:\Documents and Settings\m309112\My Documents\ESP Graduate
Schools\4-21-11\Initial_crack','lsp'
fini
/EXIT,nosav
```

### 8.1.2 Crack Growth LS001 (.macro)

```
/BATCH,LIST
/CWD,'C:\Documents and Settings\m309112\My Documents\ESP Graduate
Schools\4-21-11'
/FILNAME,'crkgrwth_STEP_001',0
/CONFIG,NOELDBW,1
/INPUT,'C:\Documents and Settings\m309112\My Documents\ESP Graduate
Schools\4-21-11\crkgrwth_STEP_001','cdb'
/PREP7
save
/COM, select everything and solve
allsel,all,all
/SOLU
eqslv,PCG,1.0e-8
/COM, input solve commands
/INPUT,'C:\Documents and Settings\m309112\My Documents\ESP Graduate
Schools\4-21-11\crkgrwth_STEP_001','lsm'
```

```
/PREP7
/FORMAT,9,G,26,15
/POST1
/GRAPHICS,off
RSYS,0
/COM, reread results
/COM, INRES,ALL
/COM, FILE,'crkgrwth_STEP_001','rst'
/COM, output displacements, temperatures, crack surface pressures to
file
/INPUT,'C:\Documents and Settings\m309112\My Documents\ESP Graduate
Schools\4-21-11\crkgrwth_STEP_001','lsp'
fini
/post1
/plns,s,eqv
```

### 8.1.3 Crack Growth LS002 (.macro)

```
/BATCH,LIST
/CWD,'C:\Documents and Settings\m309112\My Documents\ESP Graduate
Schools\4-21-11'
/FILNAME,'crkgrwth_STEP_001',0
/CONFIG,NOELDBW,1
/INPUT,'C:\Documents and Settings\m309112\My Documents\ESP Graduate
Schools\4-21-11\crkgrwth_STEP_001','cdb'
/PREP7
save
/COM, select everything and solve
allsel,all,all
/SOLU
eqslv,PCG,1.0e-8
/COM, input solve commands
/INPUT,'C:\Documents and Settings\m309112\My Documents\ESP Graduate
Schools\4-21-11\crkgrwth_STEP_001','lsm'
/PREP7
/FORMAT,9,G,26,15
/POST1
/GRAPHICS,off
RSYS,0
/COM, reread results
/COM, INRES,ALL
/COM, FILE,'crkgrwth_STEP_001','rst'
/COM, output displacements, temperatures, crack surface pressures to
file
/INPUT,'C:\Documents and Settings\m309112\My Documents\ESP Graduate
Schools\4-21-11\crkgrwth_STEP_001','lsp'
fini
/post1
/plns,s,eqv
```

## 8.2 FRANC3D Output Files for Plotting Stress Intensity Factor

### 8.2.1 Initial Crack (.sif)

```
npos  KI
0.0418109   12.8012
0.125314    12.4028
0.208642    12.0653
0.291886    11.8173
0.375096    11.6386
0.458349    11.5234
0.541811    11.4582
0.625314    11.4449
0.708642    11.4972
0.791886    11.6179
0.875096    11.8339
0.958349    12.1346
```

### 8.2.2 Crack Growth LS001 (.sif)

```
npos  KI
0.0226351   12.6358
0.0659194   13.6037
0.107215    13.6282
0.14844     13.5179
0.189578    13.3205
0.230732    13.1713
0.271919    13.0388
0.313066    12.9246
0.35417     12.813
0.395239    12.7228
0.43627     12.6403
0.477512    12.5875
0.518972    12.5507
0.560268    12.5249
0.601397    12.5104
0.642515    12.5206
0.683628    12.5636
0.724746    12.6301
0.765887    12.7692
0.807003    12.8544
0.848075    12.9458
0.889152    12.8159
0.930234    12.3913
0.975388    10.7772
```

### 8.2.3 Crack Growth LS002 (.sif)

```
npos  KI
0.0213493   14.7879
0.0631861   14.3583
0.102873    13.9592
0.141876    14.0117
0.18171     14.1539
0.221874    14.1298
```

| | |
|---|---|
| 0.262044 | 14.0363 |
| 0.301795 | 13.9228 |
| 0.341631 | 13.8332 |
| 0.381815 | 13.7473 |
| 0.421829 | 13.6735 |
| 0.46184 | 13.6018 |
| 0.501839 | 13.5417 |
| 0.541582 | 13.4944 |
| 0.581383 | 13.4757 |
| 0.621521 | 13.4606 |
| 0.661585 | 13.472 |
| 0.70156 | 13.4779 |
| 0.74175 | 13.452 |
| 0.781784 | 13.4004 |
| 0.821616 | 13.235 |
| 0.861497 | 13.2472 |
| 0.901013 | 13.3982 |
| 0.940017 | 13.3044 |
| 0.979728 | 12.6007 |